Large-amplitude internal waves observed in the Kruzenshtern Strait of the Kuril Island Chain and possible water transport and mixing

Tomohiro Nakamura[a], Yasuhiro Kawasaki[b], Tokihiro Kono[c], and Toshiyuki Awaji[d]

[a] Pan-Okhotsk Research Center, Institute of Low Temperature Science, Hokkaido University, Sapporo, 060-0819, Japan

[b] Hokkaido National Fisheries Research Institute, Fisheries Research Agency, Kushiro, 085-0802, Japan

[c] Department of Marine Biology and Sciences, School of Biological Science and Engineering, Tokai University, Sapporo, 005-8601, Japan

[d] Department of Geophysics, Graduate School of Science, Kyoto University, Kyoto, 606-8502, Japan

Key words: internal wave, water-mass transformation, tidal mixing, Kuril Straits, Sea of Okhotsk

Corresponding author: Tomohiro Nakamura (nakamura@lowtem.hokudai.ac.jp)

Abstract

Vertical sections of temperature and current velocity across the sill in the Kruzenshtern Strait were observed four times in one day in September 1997. The observations captured nonlinear internal waves near the sea surface, which are likely to be tidally generated. Two of these waves had maximum amplitudes near the surface and each contained a trapped core, suggesting that a significant volumetric flux was induced. At mid depths, isotherms moved vertically more than 50 m, which is consistent with the generation of internal lee waves. From water-mass movements, the currents are estimated to flow from the North Pacific to the Sea of Okhotsk in the temperature-minimum layer at a mean speed of 0.2–0.3 m s^{-1}. The mean flow was weaker and the oscillatory component was stronger at mid depths, with the amplitude of the latter around 0.4 m s^{-1}, leading to the above lee wave generation. Active temporal variations in potential temperature, particularly those associated with small-scale patches, suggest the occurrence of vigorous water-mass transformation. Vertical and horizontal diffusivities are estimated to be O(10^{-2} m^2 s^{-1}) and O(10^2 – 10^3 m^2 s^{-1}), respectively. Because the tidal amplitude was close to the annual minimum at the time of observation, larger-amplitude internal waves and more vigorous water-mass transformation could take place at other times of the year.

1 Introduction

The Sea of Okhotsk and the North Pacific Ocean are connected through the straits in the Kuril Island Chain (Fig. 1). Water exchange between these two basins is considered to occur mainly through the two deep straits, the Kruzenshtern Strait and the Bussol Strait. This water exchange has an important role in the formation of water masses and circulation in both basins. In the Sea of Okhotsk, winter cooling and brine rejection associated with sea ice production lead to the formation of saline water near freezing temperature over the northern shelf, which is called Dense Shelf Water (e.g., Kitani, 1973; Shcherbina et al. 2003). This water is fresher than the surrounding water at the same density because of its low temperature and is considered to be one of the major sources of fresh water in the North Pacific intermediate layer (e.g., Talley, 1991; Yasuda, 1997; Kono, 1998; Watanabe and Wakatsuchi, 1998; Itoh et al., 2003).

Besides the water exchange, strong tidal mixing in the Kuril Straits is also considered to affect both the Sea of Okhotsk and the North Pacific (Nakamura et al., 2004; 2006). The tidal mixing not only modifies water properties directly in the Kuril Straits, but it also induces an upward salt flux into the surface layer from the saltier lower layer. The subsequent transport of the saline water from the Straits to regions of sea-ice generation increases the density of the Dense Shelf Water. Both of these effects enhance the ventilation in the Sea of Okhotsk. The influence of these processes spreads over almost all of the North Pacific as the water supplied from the Sea of Okhotsk circulates in the intermediate layer. Also, Nakamura et al. sug-

gested that the dynamical adjustment processes conducted mainly through coastally trapped waves and eastward advected long-Rossby waves induce intergyre transport and modify the interior circulation, respectively. Further, Yasuda et al. (2006) suggested that with the 18.6-year period nodal tidal cycle, tidal mixing in the Kuril Straits causes bi-decadal variation in the North Pacific through the above process. (There could also be a variation with a period of about six months associated with the reduction of diurnal tides near equinoxes. Such a variation, however, has not been paid much attention, which may be partly because it should be contaminated by the seasonal variation.)

Numerical modeling and theoretical studies have shown that the diurnal tides, especially the K_1 tide, have the ability to induce vigorous mixing (Nakamura et al., 2000a; Nakamura and Awaji, 2001; 2004). The diurnal tidal flow is considerably intensified around the Kuril Straits, with a maximum flow speed of over 2 ms^{-1} (e.g., Thomson et al., 1997; Luchin report in Talley and Nagata, 1995; Kowalik and Polyakov, 1998; Nakamura et al., 2000b; Ohshima et al., 2002). The intensification is due to the effective amplification of topographically trapped waves generated by the subinertial diurnal tides, whose presence was observed by Rabinovich and Thomson (2001), in addition to the effect of topographic contraction. The resulting mixing occurs from the bottom of topographic features to the sea surface along the Kuril Island Chain and is particularly intense over sills or banks of moderate depth, where the maximum vertical diffusivity may exceed 0.1 $\mathrm{m}^2\mathrm{s}^{-1}$. In numerical simulations (Nakamura et al., 2000a; Nakamura and Awaji, 2004), the locally enhanced mixing is associated with tidally generated 'unsteady lee waves' rather than internal tides

of tidal frequency. This is because the diurnal tides are subinertial at the Kurils (so that internal tides generated by them cannot be internal gravity waves) and because unsteady lee waves are more likely to grow by superposition than internal tides. Energetic internal waves are then formed with amplitudes exceeding 100 m, resulting in wave breaking.

Observations in the Kuril Straits also supported the occurrence of strong mixing. Density or temperature fronts were observed between mixed water in the straits and water in the Sea of Okhotsk or the North Pacific (Kawasaki and Kono, 1992; Gladyshev, 1995). Kawasaki (1996) observed the presence of a large number of patches in a vertical temperature section through the Kruzenshtern Strait, which may be a manifestation of mixing. Analyses of chemical tracers also suggested the importance of diapycnal mixing (Wong et al., 1998; Aramaki et al., 2001; Yamamoto et al., 2002). Recently, diapycnal diffusivity associated with turbulent mixing was estimated around the Bussol Strait from extensive Conductivity-Temperature-Depth (CTD) observations (Ono et al., 2007) and direct turbulence microstructure measurements (Yagi and Yasuda, 2008; Itoh, 2008). The estimated diffusivity is in fact huge, and there was a site where a daily and vertically averaged value was O (10^{-2} $m^2 s^{-1}$).

Nevertheless, observations of internal waves in the Kuril Straits are, thus far, very limited. As far as we are aware, only two examples have been published in international journals: A hydrographic survey in the Kruzenshtern Strait which showed that vertical displacements whose horizontal scale corresponds to a lee wave extended from the sill top toward the sea surface (Nakamura et al., 2000a), and

satellite imagery of a solitary wave train near the Bussol Strait (Nakamura and Awaji, 2004). Such a limited number of observations of internal waves is one of the obstacles to a better understanding of the link between tides and diapycnal mixing in the Kuril Straits.

In this study, we present internal waves captured in past observational data in the Kruzenshtern Strait. The waves are likely of tidal origin, and thus the observation may provide additional support for the results of previous simulations on tidal mixing. Further, some internal waves trapped near the surface may cause water transport, whose effect has not been considered around this area. The remainder of this paper is organized as follows. A summary of the observations is described in Section 2. The internal waves near the surface are presented in Section 3, and water-mass movement and internal wave generation at mid depths are investigated in Section 4. Finally, the results are summarized in Section 5.

2 Observations

The observations were conducted around the Kruzenshtern Strait (Fig. 1) during an R/V Hokko-Maru cruise in September 1997. An observation line was set along the strait (i.e., across the sill in the strait), as shown in Fig. 1b. Temperature measurements on this line (crosses in Fig. 1b) were repeated four times during one day, using Expendable BathyThermographs (XBTs). The distance between each XBT site was set at approximately 4 km to capture internal waves of relatively small wavelengths. Horizontal current velocity was also measured with a shipboard

Acoustic Doppler Current Profiler (ADCP) during the XBT observations. Although CTD measurements were performed at both ends of the line (solid circles in Fig. 1b), we focus on the XBT and ADCP measurements here.

The durations of the four XBT observations are shown in Fig. 2c with predicted tidal elevation at the observation site. In the four XBT observations, we could see different phases of tidal flow associated with diurnal tides, which make a major contribution to the current field around the Kuril Straits. However, the amplitude of tidal elevation in the strait was almost the annual minimum at the time of the observation (Fig. 2). Further, semidiurnal tides were dominant rather than diurnal tides, which usually dominate (Fig. 2). As a result, legs 1 and 3 captured a similar tidal phase corresponding to the time when the tidal elevation increased to flood tides, whereas it decreased to ebb tides during legs 2 and 4.

Figure 3 shows vertical sections of the observed potential temperature. Although potential temperature here is calculated assuming a constant salinity value since salinity was not measured with the XBTs, the associated errors were less than 0.01 °C and are small enough for the discussion in this study.

The figure shows a typical vertical structure in the subarctic North Pacific and the Sea of Okhotsk, observed in summer: Namely, the presence of the warm surface mixed layer above the seasonal thermocline, the temperature minimum layer below (called dichothermal layer), and the local temperature maximum layer at intermediate depths (called mesothermal water). The typical difference in water-mass structure between the subarctic Pacific (the right hand side) and the Sea of Okhotsk (the left hand side) is also seen, such as the respective depths of the dichothermal

layer (shallower in the North Pacific) and the North Pacific's warmer mesothermal water. These features of the background potential temperature field are similar to those observed previously (Kawasaki and Kono, 1994; Gladyshev, 1995; Kawasaki, 1996).

Between these two basins, large temporal variations occur. The elevations and depressions of isotherms are seen near the sea surface and below the mesothermal water, where the horizontal gradient of potential temperature is relatively small. In the subsurface layer, it seems that the water-mass structure is being vigorously transformed in the strait. In the following, we first focus on the disturbances near the surface in Section 3 and will come back to the subsurface variations in Section 4.

3 Near the sea surface

3.1 Internal waves

Vertical sections of potential temperature and current velocity near the sea surface are shown in Fig. 4, together with the locations of the measurements (triangles below each panel). The current velocity is decomposed into components along and across the observation line. Positive along-line velocity is directed rightward (to the Pacific side across the sill) and positive across-line velocity goes from the front side of the figure to the reverse side (to the northeast along the sill). The figure also shows the horizontal divergence of along-line velocity, the vertical integration of which gives vertical velocity under the rigid lid approximation when the divergence

of across-line velocity is negligible.

From internal wave theories, we know that solitary waves near the sea surface in such deep water form depressions, except for very high vertical modes (Ostrovsky and Stepanyants, 1989; Helfrich and Melville, 2006; Apel et al., 2007), and that horizontally propagating internal waves that are trapped vertically, or that consist of vertical modes, propagate in the direction of the across-trough velocity and have downward (or upward) vertical velocity on the front (or the rear) side of the trough (e.g., Vlasenko et al., 2005).

Such structures are observed in Fig. 4 and are numbered from 1 to 7, with arrows showing the direction of propagation. Depressions 1, 3, 4 and 7 have structures consistent with leftward propagating waves, whereas the others are consistent with rightward propagating waves. Depressions 2 and 6 exhibit more typical structures than the others. Depression 4 resembles a kink-front rather than a depression. Depression 3 seems to have a train of waves behind the leading trough according to the ADCP velocity, although the train is not resolved by XBT observations. Similarly, depression 5 could be associated with a leading wave train in front of the observed depression at 37 km. The propagation direction of depression 7 is somewhat ambiguous from the present data. The current structure suggests that the peak of the depression is located at around 34 km and is not resolved by XBT observation. If this is the case, depression 7 is propagating leftward. The presence of almost symmetric elevations on both sides of depression 1 is a curious feature. Because solitary waves of elevation do not easily occur in this situation, one simple explanation is that one large depression is embedded in the relatively large-scale

elevation. Another interpretation is that this is a part of a nonlinear and non-stationary wave train.

In spite of the ambiguity due to the resolution of the XBT observations, the relation of the phases of isotherm displacement, along-line velocity, and approximated vertical velocity suggests that these features are horizontally propagating internal waves. It is, however, difficult to track these waves since disturbances which have sufficiently similar shapes to the identified waves in previous legs are not found in the next legs. They might be non-stationary or might have gone outside the observation section. Actually, supposing that the phase speed is around 1 m s^{-1}, waves would propagate about 20 km during the observation time interval of 6 hours, so that most waves will leave the range of the observation line before the next observation.

3.2 Bolus-like depression

Among these features, depression 6 has a shape similar to known soliton solutions, though the shape is partly due to linear horizontal interpolation in drawing the figure. In addition, it is marginally resolved by 5 or 3 XBT sites, which may allow a qualitative comparison with theoretical models. Figure 5 shows the soliton solutions superposed on a close-up of the potential temperature field around depression 6. The solutions compared are the Korteweg-de Vries (KdV) and extended KdV solitons (eKdV; e.g., reviews by Ostrovsky and Stepanyants, 1989; Helfrich and Melville, 2006; Apel et al., 2007), the Miyata soliton (Miyata, 1988; Choi and Camassa, 1999), and the JKKD soliton (Joseph, 1977; Kubota et al., 1978). Note that these are weakly nonlinear models (shallow water models), except for the Miyata soliton

(the JKKD soliton).

The solutions shown are obtained for a two layer system, in which the horizontal length scale of all solitons depends on the density and thickness of the upper and lower layers (ρ_1, ρ_2, h_1, and h_2, respectively) and soliton amplitude. When Boussinesq approximation is valid ($\rho_1 \approx \rho_2 = \rho_0$), ρ_1 and ρ_2 affect the soliton solutions through the reduced gravity acceleration, $g' = (\rho_2 - \rho_1)g/\rho_0$. The reduced gravity, however, does not affect the length scale of these solitons, as indicated in Apel et al. (2006) for the case of the KdV soliton. (This is because our results were not obtained from a mooring at a fixed point, so that there is no need to take the temporal change or the soliton speed into account.) Further, a soliton amplitude is determined by the depth of the depression at $x = 0$ km in Fig. 5, and the total depth (i.e. $h_1 + h_2$) is set to be an observed value (≈ 1700 m). We determined the remaining parameter (h_1) by doing parameter fitting, using depths of an isotherm at five XBT sites, though the outermost two have relatively little effects.

After the parameter fitting, we obtained a qualitatively similar shape as compared with observed isotherms for all of the above soliton solutions. The depths of the isotherm (thin solid line) agreed qualitatively with the soliton solutions at the XBT observation sites, although the shape of the isotherms between the XBT sites could be an artifact of linear interpolation. The JKKD soliton (dash dot) has a significantly different shape as compared with the other soliton solutions, whereas the other three soliton solutions give very similar shapes for the parameter set used here, though the Miyata soliton (thick solid line) is slightly wider than the KdV and eKdV solitons (two indistinguishable dotted lines). It should be noted, however,

that ambiguity remains in the determination of the parameter (h_1 or h_2) due to the absence of salinity and hence density distributions with depth. For example, the shape of the JKKD soliton differs further when the same set of parameters is used (short dashes). The lack of density profiles and/or the number of XBTs prevent us from making a quantitative comparison.

Interestingly, this depression has the maximum displacement near the surface and contains warm water enclosed by an isotherm and the sea surface: The maximum displacement occurs around the 7 °C isotherm, which approaches the sea surface away from the depression, whereas the seasonal thermocline is around the 3.5 °C isotherm located about at a depth of $\sim$ 40 m (Fig. 4). In contrast, weakly nonlinear waves are amenable to separation into a horizontal structure function and vertical modes, which have a maximum vertical displacement around the main pycnocline for the first mode and near the seasonal thermocline for high modes. The above feature thus suggests strong nonlinearity of the wave or that the wave is trapped very near the surface. If we assume that the latter is the case and that the main pycnocline experienced by the wave lies near the surface, the JKKD soliton alone provides a curve (long dashes) whose length scale is comparable to that of the observed isotherms. The other solutions predict much smaller length scales (not shown). The length scale of this JKKD soliton solution is, however, still shorter than that observed, which plausibly suggests that strong nonlinearity also makes a contribution.

Further, if we place it upside down, this feature is similar to internal boluses on the bottom of continental shelves, which are generated through the interaction of

incident internal waves with topography and which have been seen in observations (Klymak and Moum, 2003; Carter et al., 2005) and in numerical experiments (Venayagamoorthy and Fringer, 2006). These boluses are known to induce transport of water inside them and to provide significant bursts of turbulent kinetic energy that can contribute to diapycnal mixing, suggesting that depression 6 could have similar effects.

Also, depression 3 observed at the nearly opposite tidal phase (leg 3) has a similar bolus-like feature but with the opposite propagation direction, suggesting that such boluses are frequently generated by tides. Assuming that such boluses transport the water contained inside and that two boluses are generated in one tidal cycle (with opposite propagating directions), the volumetric flux is roughly estimated to be of the order of 0.1 Sv (1 Sv = 10^6 m^3 s^{-1}), using the estimated area contained in depression 6 of $\sim 1.5 \times 10^5$ m^2 and assuming that the length scale in the across-line direction is nearly the width of the strait (50–100 km) or that a similar size of soliton is generated over most of the sill in the Strait. Considering that this volumetric flux occurred through the top 30 m depths, the estimated amount is significant for surface water transport when compared with a previous observational estimate of 1.6 Sv taking place in the upper 600 m depths (Katsumata et al., 2001). According to their observation, the residual along-strait velocity was rather vertically uniform in the upper layer, so that it would yield a transport of about 0.08 Sv in the top 30 m. Because the flux due to such boluses takes place in the surface layer, it might have a significant impact on the supply of nutrients in the euphotic zone around the strait by spreading out the nutrient-rich water in the strait, which is in turn expected to

be supplied by tidal mixing from subsurface (Freeland et al., 1998; Nakamura and Awaji, 2004; Nishioka et al., 2007).

3.3 Possible effects of rotation

It is also interesting to note that the across-line velocity also varies in the region where the horizontally propagating waves are present. The variations have similar length scales and sometimes reach significant amplitudes compared with the along-line velocity, suggesting the possible influence of the Earth's rotation.

In fact, if the across-line velocity is caused only by an inclination of the observation line relative to a wave trough, the across-line velocity should have the same or opposite phases (i.e., 0 or 180° differences) relative to the phase of the along-line velocity. This could be the case for depressions 2, 4, and 7. Nevertheless, the across-line velocity in depression 6 has asymmetric components about the center of the trough, suggesting the influence of rotation, although the smallness of the across-velocity variation suggests that this wave is in the so-called very weak rotation regime (Grimshaw, 1985), where the rotation induces transverse velocity but does not affect the wave structure. In more detail, the effect of Earth's rotation on surface and internal wave dynamics is discussed in the review by Grimshaw et al. (1998).

4 Subsurface

4.1 Water movement

Active temporal variations also take place below the surface layer, as shown in Fig. 3. We first discuss associated water-mass movement here and then water-mass transformation and the local generation of internal waves in the following subsections. Water movement is seen as the movement of potential temperature contours or anomalies in Fig. 3. Figure 6 presents selected isotherms observed during legs 1-4 (time propagates from black, blue, green to red) in order to show such movements more clearly.

The movement of the dichothermal layer incoming from the North Pacific (the right hand side) is clearest (Fig. 6a) and can be easily seen also in Fig. 3 as the movement of cold water around 100 m depth. A closer look also reveals the oscillatory movement at mid depths (Fig. 6b,c), as illustrated by arrows. These horizontal movements are made visible because of the significant difference of water-mass structures of the North Pacific and the Sea of Okhotsk at these depths. Vertical movement rather than horizontal movement is visible below mesothermal water (Fig. 6d), where the horizontal gradient of potential temperature is relatively small.

The horizontal velocity is estimated from the above water movements to be 0.2–0.5 m s^{-1} in the dichothermal layer and 0.15–0.5 m s^{-1} at mid depths. The current is always directed from the Pacific to the Sea of Okhotsk (leftward in the figure) in the dichothermal layer, whereas it reverses direction according to the tidal phase at mid depths, with the average flow directed to the Sea of Okhotsk. These differences

in current velocity with depth indicate both the presence of vertical shear of the averaged velocity and the enhanced tidal flow at depths. Similarly, vertical velocity is estimated to be $2 \times 10^{-3} - 3 \times 10^{-3}$ m s^{-1} in the dichothermal layer and $4 \times 10^{-3} - 5 \times 10^{-3}$ m s^{-1} at mid depths.

These estimates of horizontal velocity may be confirmed by ADCP velocity, although the comparison is possible only for the dichothermal layer due to the limitation of the ADCP data. The averaged along-line ADCP velocity in the depth range of 25 to 100 m is always directed to the Sea of Okhotsk at speeds of 0.07, 0.43, 0.18, 0.33 m s^{-1} during legs 1-4, respectively. The direction and magnitude of the mean ADCP velocity agree qualitatively with the estimated along-line velocity in the dichothermal layer. Also, the movement of the cold water indicates the current is slow in the time durations between legs 1 and 2 and between legs 3 and 4, whereas it is fast in the duration between legs 2 and 3, which is roughly consistent with the time variation of the mean ADCP velocity.

The magnitude of the estimated horizontal velocity is similar to those observed by lowered ADCP measurements in the same strait (Katsumata et al., 2001). However, the direction in the dichothermal layer (or the direction of the vertical shear) is opposite. Our observation shows the flow from the Pacific to the Sea of Okhotsk, which is consistent with past qualitative investigations based on water-mass analysis (e.g., Kitani, 1973). Considering that the observation by Katsumata et al. was also conducted in summer (from 31 August to 1 September, 1999), the difference in current direction suggests the presence of large horizontal variations, such as the one associated with bi-directional mean currents induced by tides (Nakamura et al.,

2000b), or significant intra-seasonal variations in the current field.

4.2 Water-mass transformation

Figure 3 also shows the large number of patches of potential temperature anomalies, with the number increasing near the sill, and the active formation and disappearance of such patches. These facts suggest the occurrence of vigorous water-mass transformation in the strait.

In particular, we may trace two events in which a large anomaly breaks into smaller patches. As the cold dichothermal water moves leftward, the cold core initially centered around 153° 44' E and 120 m depth in leg 1 (Fig. 3a) is separated into two masses located around (153° 38' E, 150 m depth) and (153° 36' E, 100 m depth) in leg 4 (Fig. 3d), plausibly due to the combined effects of vertical displacement and vertical shear. The upward (downward) movement of the cold core during legs 1 and 2 (2 and 3) seems consistent with the divergence of the along-line velocity, and the along-line movement is also roughly consistent with ADCP velocity, though the vertical shear was not observed owing to the limitation of the ADCP observation depth. Also, relatively cold water located around 153° 38.5' E and 300–450 m depths in leg 1 seems to break into three smaller patches centered at (153° 36' E, 300 m depth), (153° 36' E, 380 m depth), and (153° 40' E, 350 m depth).

Utilizing the above tracing of patches, we made rough estimates of diffusivity from a Lagrangian viewpoint:

$$K^L = \frac{1}{2}\frac{d\Phi}{dt} \approx \frac{\Phi(t+\Delta T) - \Phi(t)}{2\Delta T},$$

where Φ is the variance of the spread of water parcels in the horizontal or vertical direction, $\Phi(t)$ and $\Phi(t+\Delta t)$ are the initial and the final variance, respectively, and ΔT is the time duration (Awaji, 1982). This parameter represents the apparent diffusivity due to the distortion of water particle distributions. We estimated K^L by assuming that the patches described above are a manifestation of water particle movement.

The calculated values of horizontal diffusivity are $K_h^L \sim 10^2$ m^2 s^{-1} and $\sim 10^3$ m^2 s^{-1} for the dichothermal layer and at mid depths, respectively. The calculated vertical diffusivity is $K_v^L \sim 0.01$ m^2 s^{-1} in the dichothermal layer. These rough estimates suggest that strong horizontal and vertical mixing (or more precisely, stirring) was taking place during the observation, leading to energetic water-mass transformation. It should be noted, however, that the estimates relied on the traceability of the patches, and we cannot reject the possibility that the changes were caused by cross-line advection from the available data. Nevertheless, the occurrence of such strong mixing or stirring is qualitatively consistent with the result of previous tidal simulations (Nakamura and Awaji, 2004) and is a likely cause of the presence of many unsteady patches.

4.3 Internal wave generation over the sill

Vertical displacement of isotherms is seen over the sill below 500 m depth in Fig. 3 and is shown for the selected isotherm in Fig. 6d. These are suggestive of internal wave generation by the flow passing over the sill.

The temporal evolution of the isotherms shown in Fig. 6d displays elevation on

the downstream side of the sill: After the current flows leftward during legs 1 and 2 as estimated from the water-mass movement (Fig. 6c), the isotherm observed at leg 2 (the blue curve in Fig. 6d) is elevated on the left hand side of the sill top (its location is indicated by the solid triangle in Fig. 6d). Similarly, the rightward (leftward) flow during legs 2 and 3 (3 and 4) produced an elevation on the right (left) hand side of the sill top, as shown by the green (red) colored isotherm. These features resemble the results of numerical experiments on unsteady lee waves rather than internal tides.

Internal waves generated by a tidal flow has intrinsic frequency approximately given by the sum or difference of Doppler shift (or lee wave frequency) and the corresponding tidal frequency, that is $-kU \pm \omega$, where k is horizontal wavenumber of generated waves or the topography, U and ω are the tidal flow speed and frequency, respectively (Nakamura et al., 2000a). Accordingly, tidally generated internal waves can be classified using the ratio, kU_0/ω, into internal tides of tidal frequency (when $kU_0/\omega \ll 1$), unsteady lee waves (when $kU_0/\omega \gg 1$), and waves in the intermediate regime referred to mixed tidal-lee waves (when $kU_0/\omega \sim 1$), where U_0 is tidal flow amplitude. This ratio is estimated to be approximately 2 in the present case, in which the horizontal scale and the flow speed are about 10 km and 0.4 m s^{-1}, respectively, and semidiurnal tides are dominant. The waves generated near the sill top are thus characterized as mixed tidal-lee waves but are close to unsteady lee waves.

The propagation and growth of unsteady lee waves are deeply affected by advection (Nakamura and Awaji, 2001). Accordingly, their co-phase lines and group

velocity are not parallel. The wave phase propagates upstream and downward, forming cophase lines slanting upstream from the vertical, whereas the wave energy is advected downstream and thus propagates almost vertically upward, moving slightly downstream (e.g., reviews by Gill, 1982; Baines, 1995 for steady lee waves and Lott and Teitelbaum, 1993; Nakamura and Awaji, 2001 for unsteady lee waves). As a result, elevation takes place immediately downstream of the sill top at a shallower depth. These features of unsteady lee waves are consistent with the observed isotherm evolution.

The effect of these internal lee waves generated over the sill would reach the surface layer by emanating wave rays. The lee wave generation by tidal flow over the sill is thus one candidate of the origin of the horizontally propagating internal waves near the sea surface.

Note that while unsteady lee waves tend to be generated near a sill top, waves generated over sill slopes usually become internal tides. This is because over sill slopes (near the sill top), the tidal flow amplitude is small (large) and the horizontal scale of the topography is large (small), so that the ratio kU_0/ω becomes small (large). The generation of internal tides is thus expected to occur over the sill slopes; however, it is difficult to extract their signal from the present data.

5 Summary and discussion

The repeated XBT and ADCP observations in the Kruzenshtern Strait revealed the presence of internal waves near the sea surface and the vertical motion of isotherms

which are consistent with the generation of internal lee waves having an amplitude of about 50 m over the sill top in the strait.

Most of the near-surface waves have such large amplitude that nonlinearity becomes important. In particular, the observation found nonlinear internal waves which seem to be trapped near the sea surface and likely carry water inside an area enclosed by the isotherm and the sea surface as they propagate. A rough estimate of the volume flux induced by such waves is O (0.1 Sv), which is a significant amount considering that it takes place in the top 30 m depths.

Considering that the propagation direction of these waves is not one sided (i.e., there were waves propagating to the Pacific side and those to the Sea of Okhotsk side), the waves are plausibly of tidal origin. However, it is difficult to determine the generation sites from the present data. Although lee waves generated over the sill in the strait are one possible origin, waves generated in the adjacent straits or the bank located around 48.2°N, 154.7°E (Fig. 1b) could come into the observation site, as seen in a numerical simulation (Fig. 9 of Nakamura and Awaji, 2004).

The currents estimated from water-mass movements always flowed from the North Pacific to the Sea of Okhotsk in the dichothermal layer at an average speed of 0.2–0.3 m s^{-1}, whereas the average flow was weaker and the oscillatory component was stronger at mid depths, with an amplitude of around 0.4 m s^{-1}. The presence of many small-scale patches in the potential temperature field and their active temporal variations suggest the occurrence of vigorous water-mass transformation. In fact, rough estimates yield vertical diffusivity of O(10^{-2} m^2 s^{-1}) in the dichothermal layer and horizontal diffusivities of O(10^2 m^2 s^{-1}) in the dichothermal layer and

$O(10^3\ m^2\ s^{-1})$ at mid depths.

Lastly, it should be noted that the present observations were conducted when the tidal amplitude was close to the annual minimum and semi-diurnal tides were dominant. Internal tides can be internal waves for semi-diurnal tides but cannot be for diurnal tides, which are subinertial around the Kuril Straits. The internal-tide response is thus expected to be different from that at the observation time and that in typical conditions in which diurnal tides dominate. However, unsteady lee waves can be internal waves even when generated by subinertial diurnal tides. Further, the behavior of unsteady lee waves is controlled by the ratio kU_0/ω rather than by the corresponding tidal frequency for the same stratification, topography, and inertial frequency. One can therefore expect, at least theoretically, to see internal lee waves of larger amplitudes and more intense water-mass transformation at other times of the year when the tidal flow is swifter and diurnal tides of smaller frequency are dominant. This should be especially so near spring tides.

Acknowledgments

We thank the two reviewers for their valuable comments. Numerical calculations were performed on the Pan-Okhotsk Information System of ILTS. One author (T.N.) was partly supported by a Grant-in-Aid for Young Scientists (KAKENHI).

References

Aramaki, T., S. Watanabe, T. Kuji, and M. Wakatsuchi, 2001. The Okhotsk-Pacific seawater exchange in the viewpoint of vertical profiles of radiocarbon around the Bussol' Strait. *Geophys. Res. Lett.*, *28*, 3971-3974.

Apel J., L. A. Ostrovsky, Y. A. Stepanyants, and J. F. Lynch, 2006. Internal solitons in the ocean. *Woods Hole Oceanogr. Inst. Tech. Rep.*, *WHOI-2006-04*, 95pp.

Apel J., L. A. Ostrovsky, Y. A. Stepanyants, and J. F. Lynch, 2007. Internal solitons in the ocean and their effect on underwater sound. *J. Acoust. Soc. Am.*, *121 (2)*, 695-722.

Awaji, T., 1982. Water mixing in a tidal current and the effect of turbulence on tidal exchange through a strait. *J. Phys. Oceanogr.*, *12*, 501-514.

Baines, P. G., 1995. *Topographic Effects in Stratified Flow*, Cambridge University Press, 498pp.

Carter, G. S., M. C. Gregg, and R.-C. Lien, 2005. Internal waves, solitary-like waves, and mixing on the Monterey Bay shelf. *Continental Shelf Res.*, *25*, 1499-1520.

Choi, W. and R. Camassa, 1999. Fully nonlinear internal waves in a two-fluid system. *J. Fluid Mech.*, *396*, 1-36.

Gill, A. E., 1982. *Atmosphere-Ocean Dynamics*, Academic Press, San Diego, 662pp.

Gladyshev, S. V., 1995. Fronts in the Kuril Island region. *Oceanology*, English translation, *34*, 452-459.

Grimshaw, R., 1985. Evolution equations for weakly nonlinear, long internal waves in a rotating fluid. *Stud. Appl. Math.*, *73*, 1-33.

Grimshaw, R.H.J., L.A. Ostrovsky, V.I. Shrira, and Y.A. Stepanyants, 1998. Long nonlinear surface and internal gravity waves in a rotating ocean. *Surv. Geophys.*, *19*, 4, 289–338.

Freeland, H.J., Bychkov, A.S., Whitney, F., Taylor, C., Wong, C.S., Yurasov, G.I., 1998. WOCE section P1W in the Sea of Okhotsk - 1. Oceanographic data description. *J. Geophys. Res.*, *103*, 15,613-15,623.

Helfrich, K. R. and W. K. Melville, 2006. Long nonlinear internal waves. *Annu. Rev. Fluid Mech.*, *38*, 395-425.

Itoh, M., K. I. Ohshima, and M. Wakatsuchi, 2003. Distribution and formation of Okhotsk Sea Intermediate Water: An analysis of isopycnal climatological data. *J. Geophys. Res.*, *108*, 3258, doi:10.1029/2002JC001590.

Itoh, S., 2008. Observations of current and turbulence within the Urup Strait. *Kaiyo Monthly*, *50*, 77-84 (in Japanese).

Joseph, R. I., 1977. Solitary waves in a finite depth fluid. *J. Phys. A Math. Gen.*, *10*, L225-L227.

Katsumata, K., I. Yasuda, and Y. Kawasaki, 2001. Direct current measurements at Kruzenshterna Strait in summer. *Geophys. Res. Lett.*, *28*, 319-322.

Kawasaki, Y. and T. Kono, 1992. Baroclinic water exchange in the Kuril Basin and the northwestern Pacific in summer. *Sea Sky*, *68*, 41-54 (in Japanese with English abstract and figure captions).

Kawasaki, Y. and T. Kono, 1994. Distribution and transport of Subarctic Waters around the middle of Kuril Islands. *Sea Sky*, *70*, 71-84 (in Japanese with English abstract and figure captions).

Kawasaki, Y., 1996. The origin of the North Pacific Intermediate Water — from the observations in the Okhotsk Sea —. *Kaiyo Mon.*, *28*, 545-552 (in Japanese).

Kitani, K., 1973 An oceanographic study of the Okhotsk Sea — particularly in regard to cold waters. *Bulletin of the Far Seas Fisheries Research Laboratory*, *9*, 45-77.

Klymak, J. M. and J. N. Moum, 2003. Internal solitary waves of elevation advancing on a shoaling shelf. *Geophys. Res. Lett.*, *30*, 2045, doi:10.1029/2003GL017706.

Kono, T., 1998 Formation of the salinity minimum in the Mixed Water Region between the Oyashio and Kuroshio Fronts. *Deep-Sea Res. Part 1*, *45*, 2035-2057.

Kowalik, Z., and I. Polyakov, 1998 Tides in the Sea of Okhotsk. *J. Phys. Oceanogr.*, *28*, 1389-1409.

Kubota, T., D. R. S. Ko, and L. D. Dobbs, 1978. Weakly-nonlinear long internal waves in a stratified fluid of finite depth. *J. Hydronaut.*, *12*, 157-165.

Lott, F., and H. Teitelbaum, 1993. Topographic waves generated by a transient wind. *J. Atmos. Sci.*, *50*, 2607-2624.

Matsumoto, K., T. Takanezawa, and M. Ooe, 2000. Ocean tide models developed by assimilating TOPEX/POSEIDON altimeter data into hydrodynamical model: A global model and regional model around Japan. *J. Oceanogr.*, *56*, 567-581.

Miyata, M., 1988. Long internal waves of large amplitude. In *Nonlinear Water Waves, IUTAM Symp., Tokyo 1987*, eds. K. Horikawa, H. Maruo, Springer-Verlag, Berlin, pp. 399-406.

Nakamura, T., T. Awaji, T. Hatayama, K. Akitomo, T. Takizawa, T. Kono, Y. Kawasaki, and M. Fukasawa, 2000a. The generation of large-amplitude unsteady lee waves by subinertial K_1 tidal flow: a possible vertical mixing mechanism in the Kuril Straits. *J. Phys. Oceanogr.*, *30*, 1601-1621.

Nakamura, T., T. Awaji, T. Hatayama, K. Akitomo, and T. Takizawa, 2000b. Tidal exchange through the Kuril Straits. *J. Phys. Oceanogr.*, *30*, 1622-1644.

Nakamura, T. and T. Awaji, 2001. A growth mechanism for topographic internal waves generated by an oscillatory flow. *J. Phys. Oceanogr.*, *31*, 2511-2524.

Nakamura, T. and T. Awaji, 2004. Tidally induced diapycnal mixing in the Kuril Straits and its role in water transformation and transport: A three-dimensional nonhydrostatic model experiment. *J. Geophys. Res.*, *109*, C09S07, doi:10.1029/2003JC001850.

Nakamura, T., T. Toyoda, Y. Ishikawa, and T. Awaji, 2004. Tidal mixing in the Kuril Straits and its impact on ventilation in the North Pacific Ocean. *J. Oceanogr.*, *60*, 411 - 423.

Nakamura T., T. Toyoda, Y. Ishikawa, and T. Awaji, 2006. Effects of tidal mixing at the Kuril Straits on the North Pacific ventilation: Adjustment of intermediate layers revealed from numerical experiments. *J. Geophys. Res.*, *111*, C04003, doi:10.1029/2005JC003142.

Nishioka, J., Ono, T., Saito, H., Nakatsuka, T., Takeda, S., Yoshimura, T., Suzuki, K., Kuma, K., Nakabayashi, S., Tsumune, D., Mitsudera, H., Johnson, W. K., Tsuda, A., 2007. Iron input into the western subarctic Pacific, importance of iron export from the Sea of Okhotsk. *J. Geophys. Res.*, *112*, C10012, doi:10.1029/2006JC004055.

Ohshima, K. I., M. Wakatsuchi, Y. Fukamachi, and G. Mizuta, 2002. Near-surface circulation and tidal currents of the Okhotsk Sea observed with the satellite-tracked drifters. *J. Geophys. Res.*, *107*: art. no. 3195.

Ono, K., K. I. Ohshima, T. Kono, M. Itoh, K. Katsumata, Y. N. Volkov, and M. Wakatsuchi, 2007. Water mass exchange and diapycnal mixing at Bussol Strait revealed by water mass properties *J. Oceanogr.*, *63*, 281-291.

Ostrovsky, L. A. and Y. A. Stepanyants, 1989. Do internal solitons exist in the ocean? *Rev. Geophys.*, *27*, 293-310.

Rabinovich, A. B. and R. E. Thomson, 2001. Evidence of diurnal shelf waves in

satellite-tracked drifter trajectories off the Kuril Island. *J. Phys. Oceanogr.*, *31*, 2650-2668.

Shcherbina, A. Y., L. D. Talley, D. L. Rudnick, 2003. Direct observations of North Pacific ventilation: Brine rejection in the Okhotsk Sea. *Science*, *302*, 1952-1955.

Talley, L. D., 1991. An Okhotsk Sea water anomaly: implications for ventilation in the North Pacific. *Deep-Sea Res.*, *38*, s171-190.

Talley, L. D. and Y. Nagata, 1995. *The Okhotsk Sea and Oyashio region.* PICES Scientific Report No. 2, Sidney, B. C., Canada., 227pp.

Thomson, R. E., P. H. LeBlond, and A. B. Rabinovich, 1997. Oceanic odyssey of a satellite-tracked drifter: North Pacific variability delineated by a single drifter trajectory. *J. Oceanogr.*, *53*, 81-87.

Venayagamoorthy, S. K. and O. B. Fringer, 2006. Numerical simulations of the interaction of internal waves with a shelf break. *Phy. Fluids*, *18*, 076603.

Vlasenko, V., N. Stashchuk, and K. Hutter, 2005. *Baroclinic tides. Theoretical modeling and observational evidence*, Cambridge University Press, Cambridge.

Watanabe, T., and M. Wakatsuchi, 1998. Formation of 26.8 σ_θ water in the Kuril Basin of the Sea of Okhotsk as a possible origin of North Pacific Intermediate Water. *J. Geophys. Res.*, *103*, 2849-2865.

Wong, C. S., R. J. Matear, H. J. Freeland, F. A. Whitney, and A. S. Bychkov,

1998. WOCE line P1W in the Sea of Okhotsk 2. CFCs and the formation rate of intermediate water. *J. Geophys. Res.*, *103*, 15,625-15,642.

Yagi, M. and I. Yasuda, 2008. Turbulence observation in Kuril Straits using density inversions. *Kaiyo Mon.*, *50*, 85-92 (in Japanese).

Yamamoto, M., S. Watanabe, S. Tsunogai, and M. Wakatsuchi, 2002. Effects of sea ice formation and diapycnal mixing on the Okhotsk Sea Intermediate Water clarified with oxygen isotopes. *Deep-Sea Res. I*, *49*, 1165-1174.

Yasuda, I., 1997. The origin of the North Pacific intermediate water. *J. Geophys. Res.*, *102*, 893-910.

Yasuda, I., S. Osafune, and H. Tatebe, 2006. Possible explanation linking 18.6-year period nodal tidal cycle with bi-decadal variations of ocean and climate in the North Pacific. *Geophys. Res. Lett.*, *33*, L08606, doi:10.1029/2005GL025237.

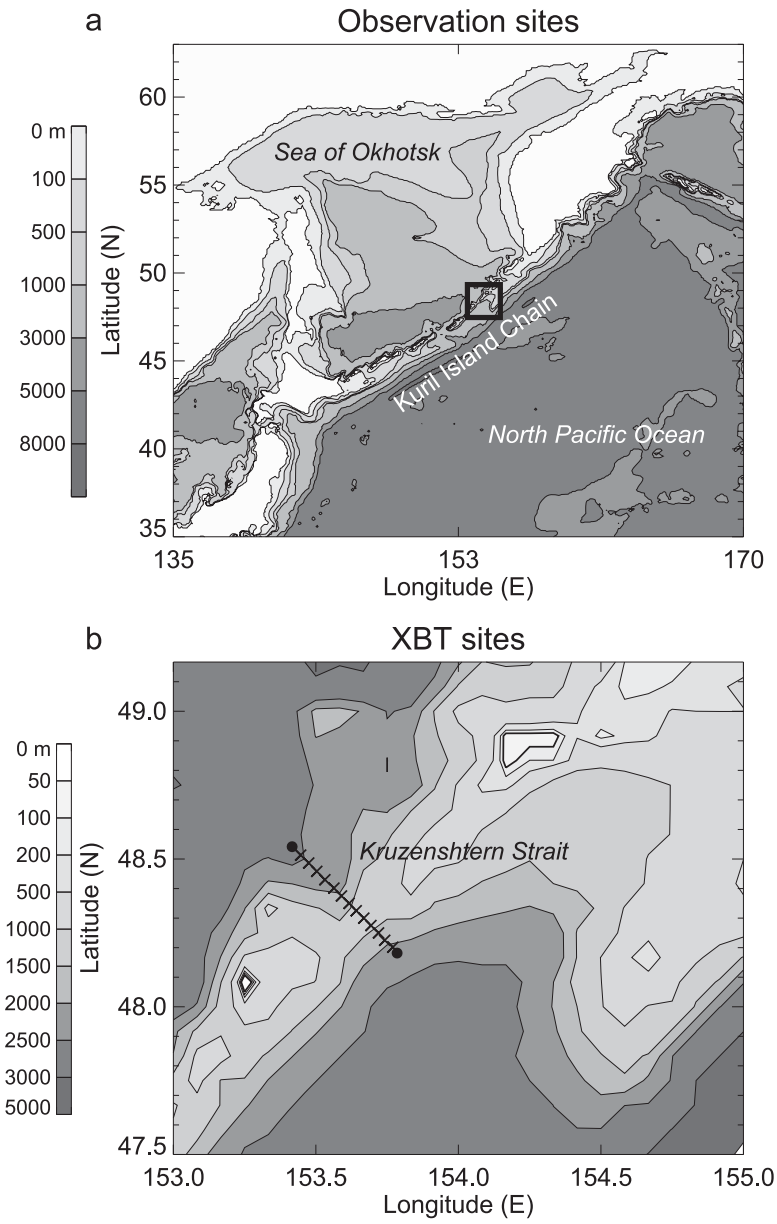

Figure 1: Observation sites. (a) Location of the Kruzenshtern Strait and the Kuril Island Chain. (b) Observation sites and topography. Crosses and solid circles indicate the sites of XBT and CTD measurements, respectively.

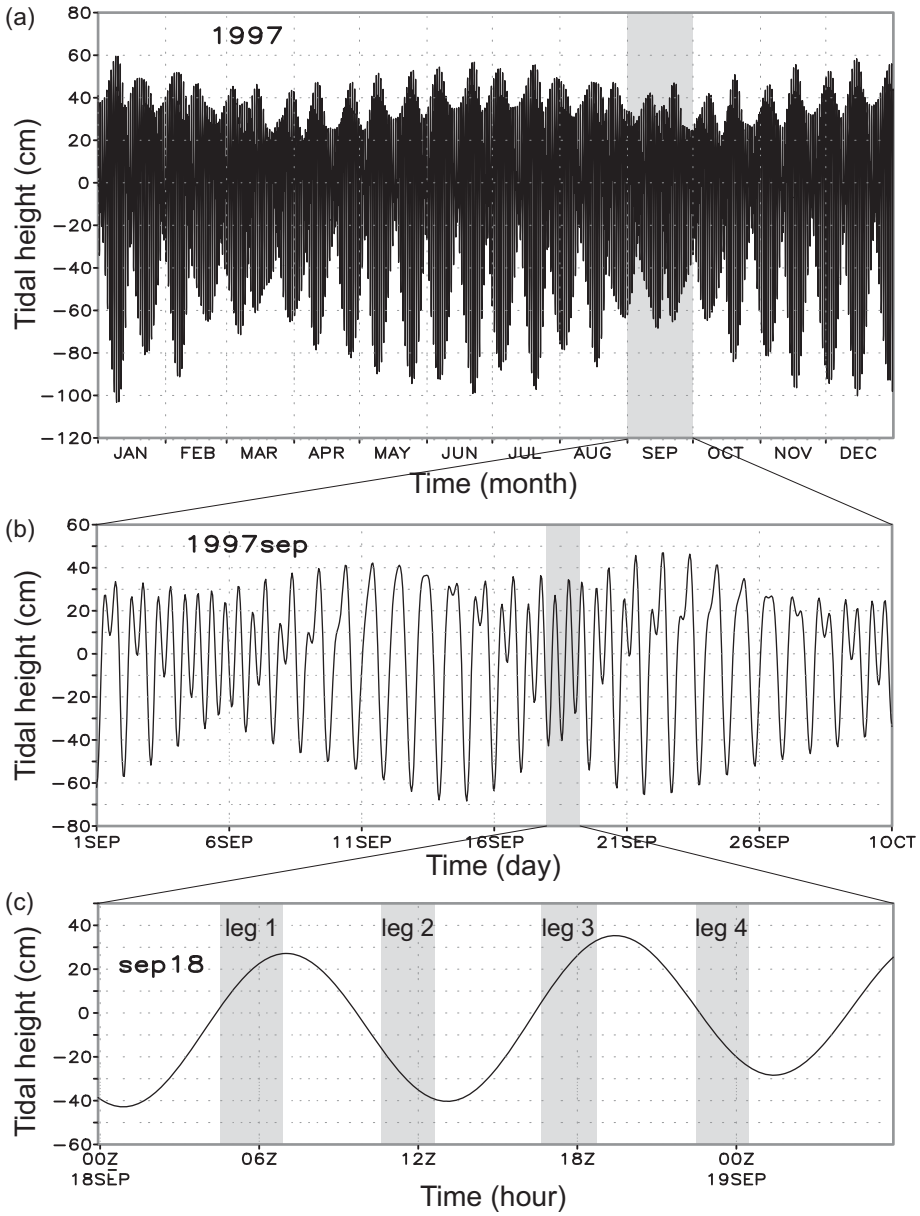

Figure 2: The time duration of the observation and tidal height during (a) 1997, (b) September 1997, and on (c) 18–19 September 1997. Shaded areas in the bottom panel show the observation duration. Tidal height is calculated based on Matsumoto et al. (2000) at the location of the sill on the observation line.

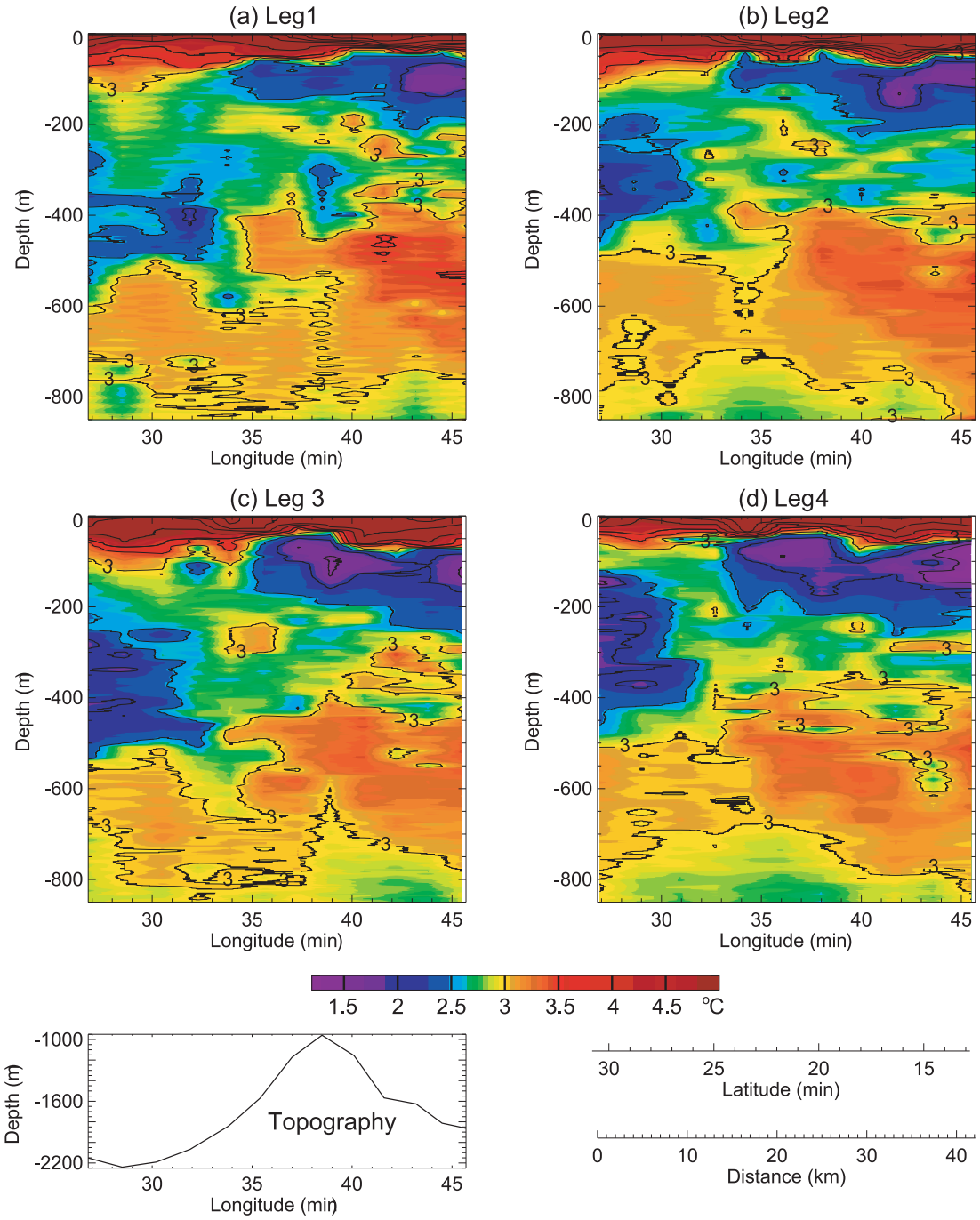

Figure 3: Vertical sections of potential temperature and the bottom topography along the observation line. Contour intervals are 0.5 °C for $\leq$ 3°C and 1°C for $>$ 3°C. The North Pacific Ocean (the Sea of Okhotsk) is on the right (left) hand side.

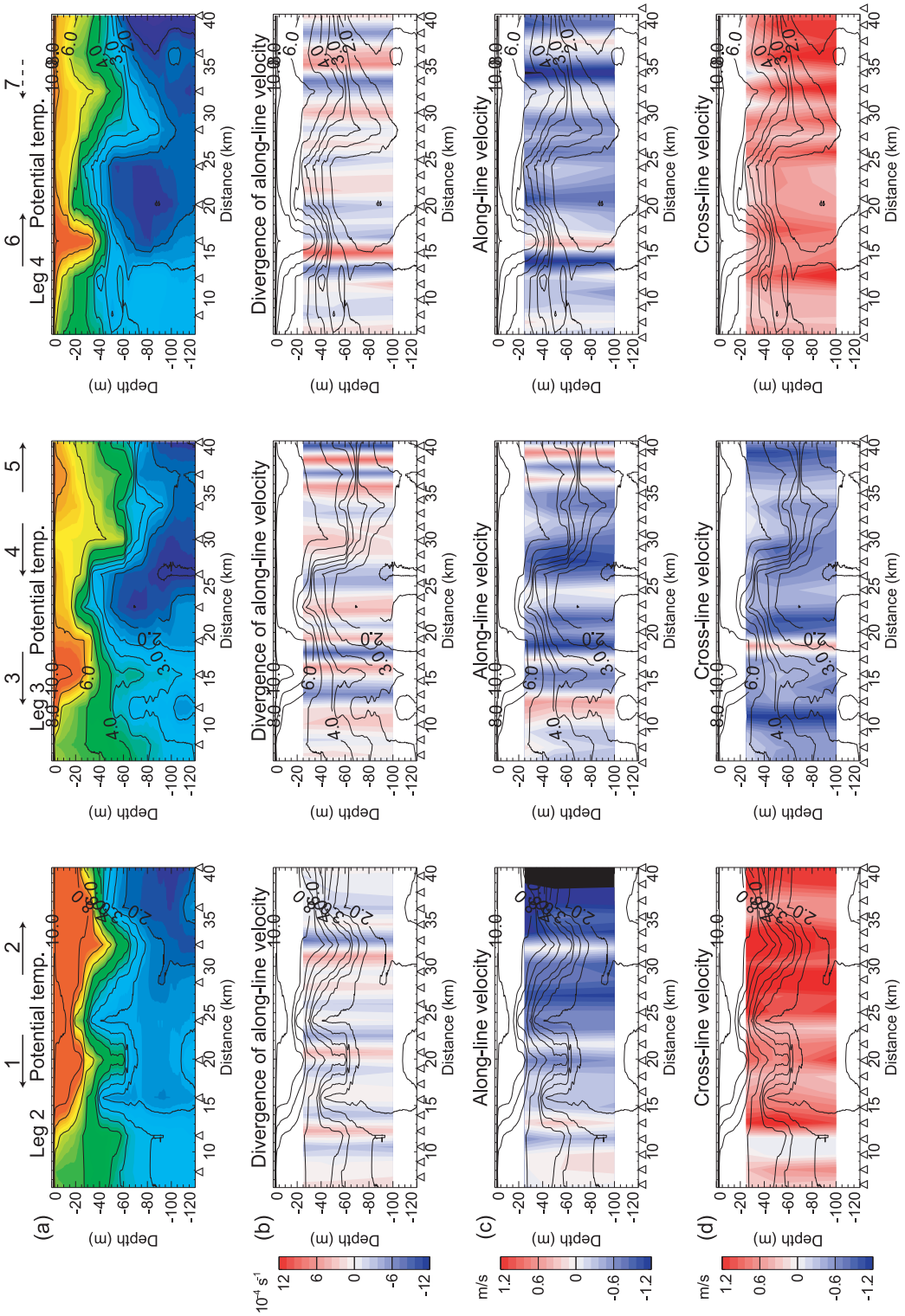

Figure 4: Vertical sections of (a) potential temperature, (b) divergence of along-line velocity, (c) along-line velocity, and (d) cross-line velocity observed in legs 2 to 4 from left to right. Triangles below each panel indicate the locations of measurements.

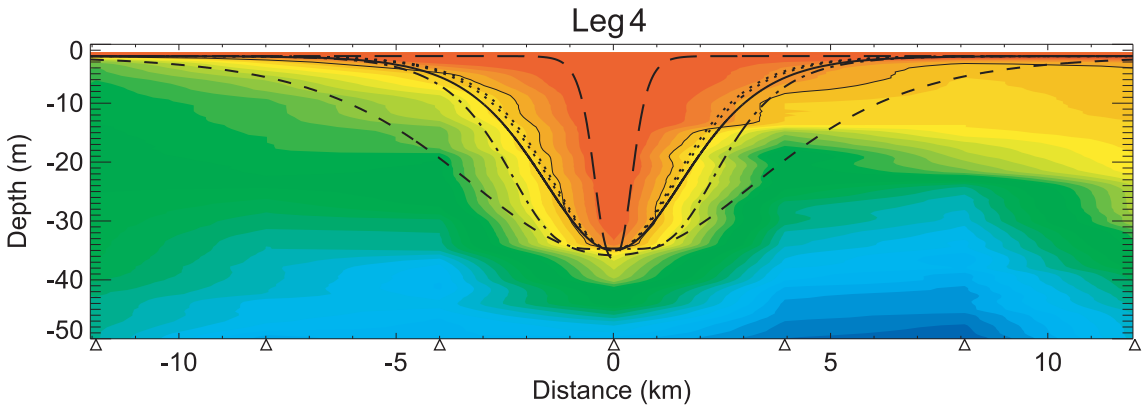

Figure 5: Comparison of the observed isotherm depression 6 in Fig. 4 and solutions of Miyata soliton (thick solid line), KdV and eKdV solitons (dotted line), and JKKD soliton (short dashed line), using parameter values selected so as to fit the former three soliton solutions to the shape of the isotherms ($h_1 = 240$ m where h_1 corresponds to the upper layer thickness in a two-layer fluid system). The KdV and eKdV soliton solutions are indistinguishable in this figure. Also shown are a JKKD soliton (dash dot) which is fitted to the isotherm shape ($h_1 = 60$ m) and a JKKD soliton (long dash) which is obtained by assuming that the pycnocline experienced by the wave lies close to the sea surface ($h_1 = 15$ m).

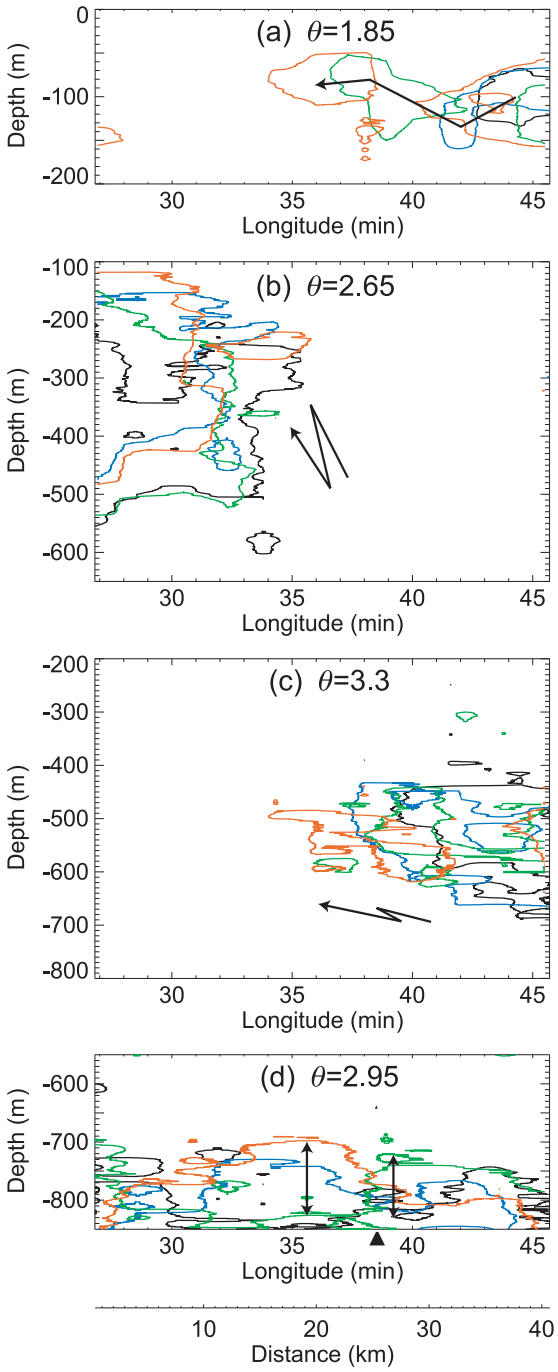

Figure 6: Isotherms selected to show the movements of water masses. Black, blue, green and red contours represent isotherms observed in legs 1 to 4, respectively. The solid triangle below the panel (d) indicates the location of the sill top.